Carbon Nanotubes Conjugated with Triazole-Based Tetrathiafulvalene-Type Receptors for C_{60} Recognition

Jaime Mateos-Gil,[†[a,b]] Joaquín Calbo,[†[c]] Laura Rodríguez-Pérez,[[a]] Mª Ángeles Herranz,*[[a]] Enrique Ortí,*[[c]] and Nazario Martín*[[a,d]]

† *These authors contributed equally to this work*

Abstract: Fullerene receptors prepared by a twofold Cu^{I}-catalyzed azide-alkyne cycloaddition (CuAAC) reaction with π-extended tetrathiafulvalene (exTTF) have been covalently linked to single-walled carbon nanotubes (SWCNTs) and multi-walled carbon nanotubes (MWCNTs). The nanoconjugates obtained were characterized by several analytical, spectroscopic and microscopic techniques (TEM, FTIR, Raman, TGA and XPS), and evaluated as C_{60} receptors by UV-Vis spectroscopy. The complexation between the exTTF-triazole receptor in the free state and C_{60} was also studied by UV-Vis and ^{1}H NMR titrations, and compared with analogous triazole-based tweezer-type receptors containing the electron-acceptor 11,11,12,12-tetracyano-9,10-anthraquinodimethane (TCAQ) and benzene rings instead of exTTF motifs, providing in all cases very similar values for the association constant (log K_a ≈ 3.0–3.1). Theoretical density functional theory (DFT) calculations demonstrated that the enhanced interaction between the host and the guest upon increasing the size of the π-conjugated arms of the tweezer is compensated by an increase in the energy penalty needed to distort the geometry of the host to wrap C_{60}.

Introduction

The discovery of fullerenes and carbon nanotubes (CNTs) expanded the family of carbon nanostructures three decades ago.[1] Both nanomaterials are extreme cases demonstrating that the electronic currents can survive even upon drastic distortion from planarity.[2] Besides the singular shape and geometry of these carbon nanostructures, their mechanical, thermal and optoelectronical properties have aroused a huge interest for applications in different fields such as organic electronics and drug delivery.[3]

Many efforts have been invested for improving the low solubility of fullerenes and CNTs, and to modulate their intrinsic properties by means of different chemical strategies, either by covalent and non-covalent methods.[4] Whereas the non-covalent functionalization of fullerenes and CNTs endows them with a suitable solubility while preserving their major structural characteristics, the covalent functionalization entails the saturation of some of the sp^2 carbons forming their π-conjugated structure. As expected, the stability of the non-covalent hybrids is significantly influenced by the experimental conditions (solvent, pH, temperature, etc.), whereas the covalent functionalization results in more stable products.[5]

Within the different strategies to functionalize fullerenes, one of the most challenging research topics has been the development of suitable receptors or hosts that, on the basis of non-covalent bonding, are able to recognize selectively different fullerene sizes or different fullerenes from carbon soot.[6] Several motifs and structures have been reported to strongly associate with fullerenes by establishing π–π, CH−π, and electrostatic interactions or coordination bonds. Planar molecules such as porphyrins have been employed as popular receptors,[7] even though their planar structure do not match the curved geometry of fullerenes, thus diminishing the association constants and the through-space electronic communication. Bowl-shaped π-conjugated molecules such as subphthalocyanines,[8] subporphyrins,[9] modified truxenes, and corannulenes[10] have also been investigated as fullerene receptors. However, their relatively weak electron-donating properties compared with those of porphyrins usually require the presence of additional substituents in order to increase their binding ability toward fullerenes in solution. The development of tweezer,[11] box/ring,[12] and cage hosts [13] has resulted in receptors with a high affinity and good selectivity towards certain fullerene homologues.

Following the tweezer-type strategy, 9,10-bis(1,3-dithiol-2-ylidene)-9,10-dihydroanthracene (exTTF) derivatives were investigated as recognizing motifs for fullerenes.[14] In these systems, besides π–π and charge-transfer interactions, a specific contribution to the overall stabilization of the complex arosing from the concave-convex pairing between exTTF and fullerenes has been validated.[15]

On the basis of this background, the aim of this work was to study the behavior of a tweezer-like receptor based on exTTF as recognition motif for C_{60} when covalently supported on CNT surfaces. These carbon nanotube-C_{60} nanohybrids were assembled in a tricomponent electroactive system with the aid

a] *Dr. J. Mateos-Gil, Dr. L. Rodríguez-Pérez, Dr. M. A. Herranz, Prof. Dr. Nazario Martín*
Departamento de Química Orgánica, Facultad de Química
Universidad Complutense de Madrid
28040 Madrid (Spain)
E-mail: maherran@ucm.es, nazmar@ucm.es
[b] *Dr. J. Mateos-Gil current address:*
Stratingh Institute for Chemistry,
University of Groningen,
Nijenborgh 4, 9747 AG, Groningen (The Netherlands)
[c] *Dr. J. Calbo, Prof. Dr. E. Ortí*
Instituto de Ciencia Molecular
Universidad de Valencia
46980 Paterna (Spain)
E-mail: enrique.orti@uv.es
[d] *Prof. Dr. Nazario Martín*
IMDEA-Nanociencia, c/Faraday 9, Campus Cantoblanco,
28049 Madrid (Spain)

Supporting information for this article is given via a link at the end of the document.

of covalent and non-covalent methodologies. The CNT-exTTF tweezer nanoconjugates were synthesized by a well established methodology in the covalent chemistry of carbon nanoforms that combines arylation under Tour conditions and Cu^{I}-catalyzed azide-alkyne cycloaddition (CuAAC) reactions.[16] The host−guest complexes formed between the CNT-exTTF tweezer and C_{60} were investigated by UV−Vis spectroscopy. In order to unveil the interactions involved in the formation of the host-fullerene complex, the complexation of C_{60} with the exTTF tweezer receptor, as well as two analogous systems that contain a 11,11,12,12-tetracyano-9,10-anthraquinodimethane (TCAQ)[17] and benzene as recognition motifs instead of exTTF, was studied by ^{1}H NMR titrations and theoretical calculations.

Results and Discussion

Synthesis and characterization of CNT-based receptors

The preparation of single-walled carbon nanotubes (SWCNTs) and multi-walled carbon nanotubes (MWCNTs)-based receptors for C_{60} started with the synthesis of the exTTF tweezer receptor **4**, achieved by a Cu^{I}-catalyzed 1,3-dipolar cycloaddition followed by the conversion of the chloride **3** to the final azide (Scheme 1). The reaction of 3,5-bis(propargyloxy)benzyl chloride **1**[18] and the azido-containing exTTF **2**[19] proceeded under standard conditions,[20] in very low yields due to the precipitation of the monoaddition intermediate. The use of DMSO under microwave irradiation allowed to keep the intermediate solubilized during the reaction, and to synthesize chloride **3** with a 65% yield.

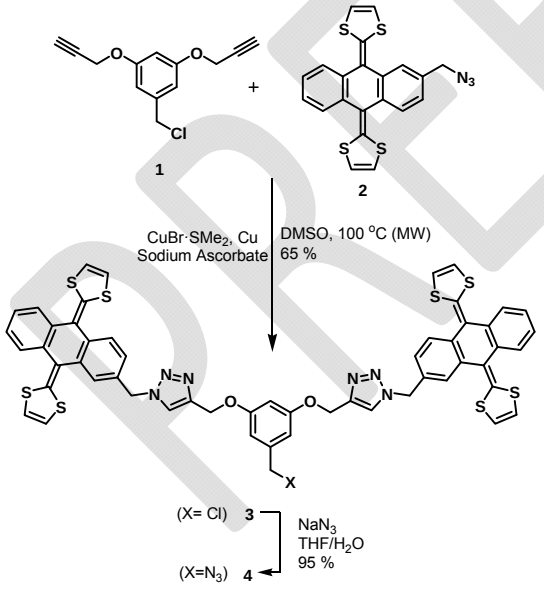

Scheme 1. Synthesis of the exTTF-triazole tweezer **4**.

Once compound **4** was synthesized, CNT endowed with protected allkyne functionalities (**SWCNT-1** and **MWCNT-1**), previously obtained by following a Tour arylation reaction,[16] were suspended in *N*-methyl-2-pyrrolidone (NMP) and reacted with tetrabutylammonium fluoride (TBAF) to deprotect the alkyne groups, which were subsequently reacted with **4** in a new Cu^{I}-catalyzed 1,3-dipolar cycloaddition process (Scheme 2).

The CNT-2-based nanoconjugates (**SWCNT-2** and **MWCNT-2**) were characterized by different microscopic, spectroscopic, and analytical techniques. The nanoconjugates morphology was investigated by TEM and did not reveal significant differences from the starting materials (Figure S1). For instance, **SWCNT-2** are observed as bundles of large diameters, coexisting with individual nanotubes disentangled by the covalent modifications performed.

FTIR spectra showed the appearance of the stretching mode of the alkyne functional group (2156–2159 cm^{-1}) of **SWCNT-1** and **MWCNT-1**, and the consecutive disappearance after the CuAAC cycloaddition to afford **SWCNT-2** and **MWCNT-2** (Figure S2 shows the evolution for the SWCNT samples). The band due to the C=C skeletal in-plane vibrations of CNT were discerned at 1597 cm^{-1} for **SWCNT-2** and at 1585 cm^{-1} for **MWCNT-2**. The presence of aliphatic C−H stretching modes, due to defects or rim terminations, are located between 2950 and 2850 cm^{-1}, the corresponding C−H bending modes at around 1250–1100 cm^{-1}.

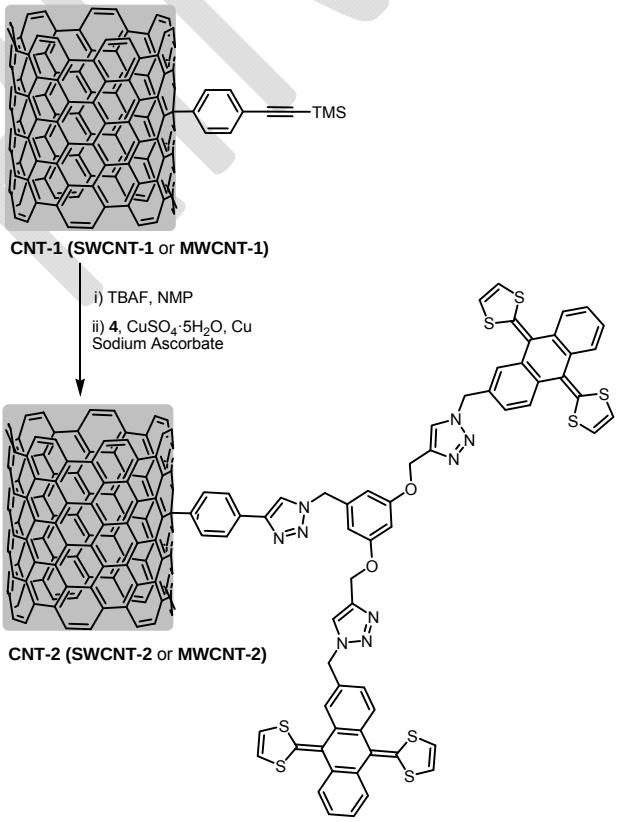

Scheme 2. Synthetic route towards CNT-2 (**SWCNT-2** and **MWCNT-2**) functionalized with exTTF-triazole tweezers through a CuAAC click chemistry approach.

Raman spectroscopy complemented the data obtained from the FTIR. For **SWCNT-2** (Figure 1), the radial-breathing-mode (RBMs) bands between 186 and 270 cm^{-1} are related to the diameter and chirality of the SWCNT, and indicate the presence

of both metallic and semiconducting SWCNT and a range of diameters between 0.8 and 1.5 nm. Furthermore, the two characteristic bands of carbon nanotubes were observed in the Raman spectra of **SWCNT-2** (Figure 1) and **MWCNT-2** (Figure S3): the D mode (sp^3 carbons; i.e., defect band) located at *ca.* 1300 cm^{-1}, due to disorder on the carbon hexagonal lattice of the CNT sidewalls, and the G mode, which corresponds to the stretching mode in the graphite (sp^2 carbons). For **SWCNT-2**, the two components of the G band are distinguished: G^+ (1594 cm^{-1}) associated with the longitudinal optical phonon mode, and G^- (1564 cm^{-1}) related with vibrations of carbon atoms along the circumferential direction of the SWCNT. In addition, the overtone mode G' related to the D band was observed in SWCNT and MWCNT samples (Figure 1 and Figure S3).[21] For these samples, the intensity ratio between the D and G bands, I_D/I_G ratio, increases significantly as a consequence of the formation of sp^3 carbons upon covalent functionalization (0.064 for pristine SWCNT, and 0.283 for **SWCNT-1** and **SWCNT-2**). The I_D/I_G ratio increases only slightly from MWCNT to **MWCNT-2** (Figure S3).

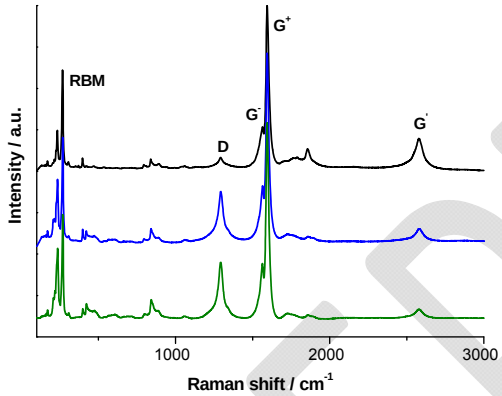

Figure 1. Comparative Raman spectra of SWCNT nanoconjugates: pristine SWCNT (black), **SWCNT-1** (blue), and **SWCNT-2** (green), obtained with an excitation wavelength of 785 nm.

Thermogravimetric analysis (TGA) measurements were performed in order to evaluate the degree of functionalization (Figures S4 and S5). As expected, a higher degree of functionalization was obtained for **SWCNT-1** when compared to **MWCNT-1**.[16] In contrast, a similar weight loss is observed in **MWCNT-2** compared to **SWCNT-2** under the same experimental conditions, what involves a better efficiency in the CuAAC of MWCNTs. This finding may be rationalized by two main reasons. For SWCNTs, the higher degree of functionalization in **SWCNT-1** implies a closer distance between alkyne functional groups that may hinder the consecutive addition of the exTTF-triazole tweezer **4** to the nanotube surface, thus decreasing the efficiency of the CuAAC reaction. For MWCNTs, the better solubility of MWCNTs favors the reaction. The total decomposition due to the **SWCNT-2** functionalization was 40%, which shows a 15% increase compared to **SWCNT-1**. For **MWCNT-2**, the weight loss is 41% (49% total weight loss).

The analyses performed by X-ray photoelectron spectroscopy (XPS) allowed the observation of the elements present in the samples (Figure 2 and S6). The recorded spectra for **SWCNT-2** and **MWCNT-2** exhibit the corresponding signals for carbon (284.6 eV), oxygen (532.6 eV), nitrogen (399.6 eV), and sulphur (169.6 eV). The contribution of the different kind of carbon atoms was evidenced after deconvolution of the C 1s core level contribution (C sp^2 and C sp^3, C=O, C−O, C−N and $\pi-\pi^*$ shake up).[22] In a similar manner, the two different contributions to the N 1s energy level signal for **SWCNT-2** and **MWCNT-2** corroborated the formation of the triazole rings as a consequence of the CuAAC reaction.[23] The peak corresponding to the S 2p at 170 eV was an evidence of the presence of the exTTF motifs.[16]

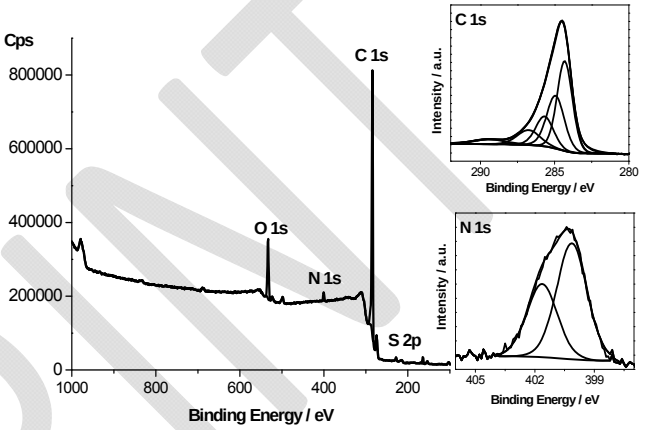

Figure 2. XPS survey spectrum of **MWCNT-2**. Insets depict the C 1s and N 1s components deconvolutions.

Complexation studies

Nanoconjugates **SWCNT-2** and **MWCNT-2** are suitable host candidates to recognize fullerenes since they bear exTTF-triazole-based molecular tweezers. Prior to the investigation of the complexation ability of these nanomaterials, the ability of the free receptor **4** to recognize C_{60} was tested in solution UV-Vis titration experiments (for experimental details, see the Supporting Information).

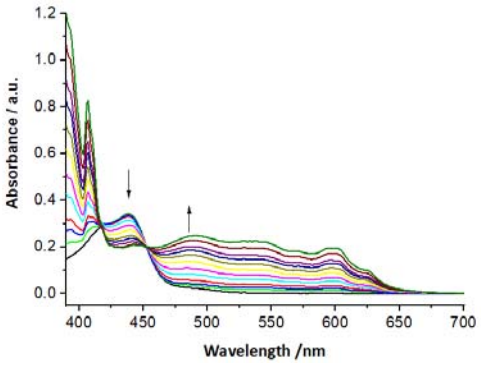

Figure 3. UV-Vis titration of a PhCl solution of **4** by addition of C_{60} (from 0 to 14 equivalents.

Quantitative measurements were performed by monitoring the changes in the UV-Vis spectra of receptor **4** (1.75×10^{-5} M) in chlorobenzene (PhCl) upon addition of C_{60} (Figure 3). The

decrease of the maximum at 438 nm is accompanied by the emergence of the well established charge-transfer band associated to tweezer exTTF•C_{60} complexes at 480 nm.[14a] Moreover, the appearance of an isosbestic point at 460 nm is suggestive of a 1:1 stoichiometry, as previously observed in other exTTF-based receptors.[14] To determine the association constant (K_a), the corrected absorbances at 438 nm were plotted and exhibit a sigmoidal pattern, which was consequently fitted to Hill's equation obtaining the better result for a Hill coefficient of n_H = 1.4 and log K_a = 3.51 (Figure S7).[14a] This sigmoidal pattern, and the interaction coefficient reflected in n_H, might be an indication of cooperativity between the different binding sites of exTTF in the formation of the complex or the evidence of remarkable conformational changes in the tweezer structure upon binding to C_{60} (see theoretical section for further details).[24] The construction of the corresponding Job's plot supports a 1:1 binding stoichiometry between **4** and C_{60}, with a maximum centered at a molar ratio of 0.5 (Figure S7).

Subsequent investigations were carried out in titrations using **SWCNT-2** and **MWCNT-2** as hosts. The hosts (2 mg) were suspended in *o*-dichlorobenzene (*o*DCB) and sonicated during 30 min to improve the nanoconjugates disaggregation. A C_{60} (1×10^{-5} M) stock solution in the same solvent was utilized for carrying out the additions.

In the case of **SWCNT-2**, the SWCNT absorption precluded the observation of the band peaking at 438 nm associated with the exTTF unit. However, the presence of an isosbestic point at 630 nm and the decrease of the SWCNT absorption upon addition of C_{60}[25] might be an indication of the formation of the supramolecular complex between **SWCNT-2** and C_{60} (Figure 4, bottom).

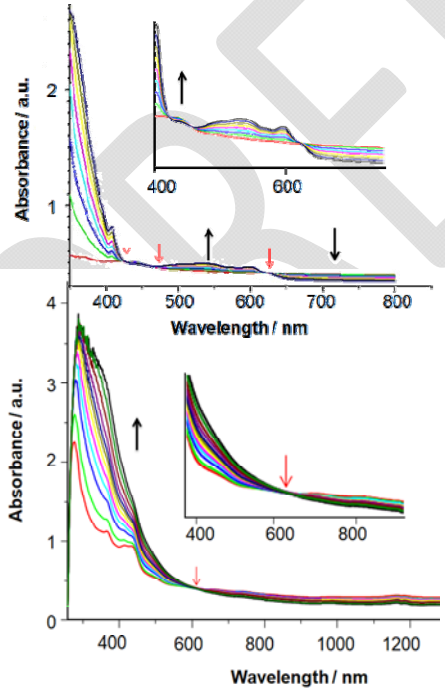

Figure 4. UV-Vis spectral changes of hosts **MWCNT-2** (top) and **SWCNT-2** (bottom) upon addition of C_{60}. Black arrows indicate the increase or the decrease in intensity of the absorption bands. Red arrows indicate the presence of isosbestic points.

The titration of **MWCNT-2** with C_{60} showed a similar behaviour: a decrease in the MWCNT absorption over 650 nm, with an isosbestic point at 630 nm (Figure 4, top). Nevertheless, the MWCNT lower absorption compared to SWCNT allowed the observation of a decrease in the intensity of the exTTF absorption at λ = 438 nm, accompanied by the increase of a broad band in the 475–600 nm region, which matches the charge transfer from exTTF to C_{60} observed in analogous molecular systems.[14,20] Therefore, the formation of the supramolecular complex not only affects the absorption features of C_{60} and exTTF, but also those of MWCNT and SWCNT, resulting in a decrease of their absorbances and the formation of new isosbestic points upon the addition of C_{60}.

With the aim of deepening the knowledge of the host-guest interactions involved in the overall stability of the triazole tweezer-C_{60} complexes, we designed and synthesized two close analogues of host **4** in which the size, geometry, and electronic character of the recognizing units were selectively tuned. As shown in Figure 5, receptors **5** and **6** preserve the central scaffold and change the exTTF units by TCAQ or benzene.

Receptor **6** was synthesized following a previously reported method.[18] For the synthesis of receptor **5**, 2-azidomethyl-9,10-bis-(dicyamomethylen)anthracene was obtained by Lehnert's condensation[26] of malononitrile and 2-(azidomethyl) anthraquinone.[27] The reaction of 3,5-bis(propargyloxy)benzyl chloride **1**[18] and the azido-containing TCAQ proceeds via a Cu^I-catalyzed 1,3-dipolar cycloaddition under similar conditions to those used for the synthesis of receptor **4** (see the Experimental Section for details).

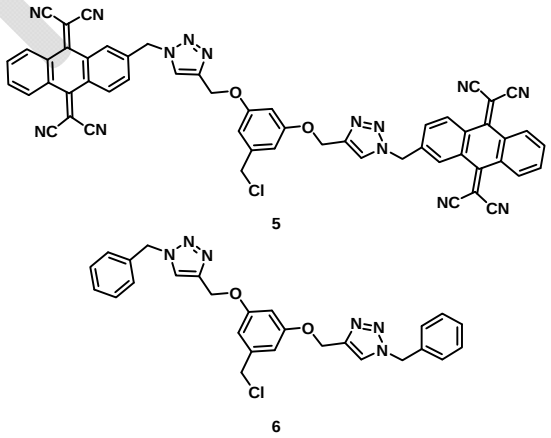

Figure 5. Chemical structures of receptors **5** and **6**.

^{1}H NMR titration experiments of receptors **4-6** with C_{60} were accomplished in order to evaluate the structural motifs that play a key role in the formation of the complexes and to estimate the values of the corresponding binding constants. The titration experiments were accomplished by using a solution of the host **4–6** (4.0×10^{-4} M) in a $CDCl_3/CS_2$ mixture, and utilizing this solution as solvent for C_{60} (3.4×10^{-3} M) in order to keep constant the concentration of the host. Limitations in the solubility of the triazole-based receptors and C_{60} prevented to reach complete saturation of the system in the titrations,

providing some degree of uncertainty in the calculated binding constants. However, the estimated values are in the range of log $K_a \approx 3.0–3.1$, as expected for these type of receptors and suitable for performing comparative analyses.

In the titration of **4**, the signals corresponding to the central benzene ring protons in the tweezer, and to the protons at positions C1, C3 and C4 of the anthracene skeleton (ring closest to triazole) of exTTF, exhibited the highest shifts (up to 0.025 ppm). In contrast to the protons of the 1,3-dithiole rings, which remain mostly unaltered, the proton in the triazole ring and the aromatic signals of the protons at positions C5, C6, C7 and C8 of the anthracene skeleton of exTTF also exhibited observable shifts (Figures S8–S12). A remarkable feature in the titration is the change in the doublet of doublets (*dd*) signal at 7.18 ppm for the proton at position C3 of the anthracene skeleton of exTTF, which decreased at the time that a new singlet appears at 7.36 ppm (Figure 6) in a slow rate exchange in the NMR time scale. The observed shifts were plotted and fitted (see details in the Supporting Information), affording similar values for all the considered signals, with an average value for log K_a = 3.1 (Table S1, Figure S13).

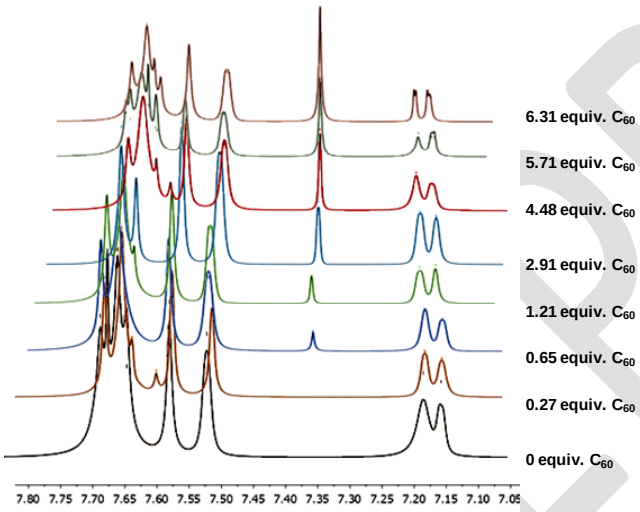

Figure 6. ^{1}H NMR titration experiment for system **4**•C_{60} enhancing the changes in the 7.18 ppm *dd* signal of the anthracene skeleton and the appearance of a new singlet at 7.36 ppm. The signal of $CDCl_3$ has been suppressed for clarity.

Compared with a family of previously reported tweezers in which the two exTTF or TCAQ units were directly attached to a central isophthalic diester moiety,[15] the new receptors **4** and **5** bear a larger central platform and were expected to show an enhanced fullerene recognition ability. However, the log K_a values estimated for **4**–**5**•C_{60}, in the range of 3.05–3.12, are similar to those previously obtained (log K_a = 2.90–3.48). As discussed below on the basis of theoretical calculations, the extension of the central core not only promotes a larger amount of noncovalent interactions but also gives additional flexibility to the tweezer, which may result in larger deformation energies, thus balancing the net C_{60} affinity.

The ^{1}H NMR signals of **5** upon increasing C_{60} addition revealed observable shifts in the triazole (7.95 ppm), central phenyl ring (6.62 and 6.58 ppm) and CH_2Cl (4.48 ppm) signals (Figures S14–S17). On the other hand, very small changes were observed in the signals assigned to the anthracene skeleton of TCAQ (Figures S18–S19). The singlet signal corresponding to the methylene group between the TCAQ unit and the triazole remained almost unaltered, but the other methylene group, close to the central ring, showed a small shift. The data fitting revealed very similar values for the association constant to those obtained for **4•C$_{60}$** (Table S1, Figure S20).

The ^{1}H NMR titration of host **6** with increasing amounts of C_{60} revealed the same tendency, demonstrating observable shifts in the triazole (7.55 ppm), central phenyl ring (6.60 and 6.54 ppm), and CH_2Cl (4.46 ppm) signals, whereas the side phenyl rings signals were almost unaltered (Figures S21–S24). The data fitting yield results in the same line than for the other two studied systems (Table S1, Figure S25).

In view of the obtained results, the triazole ring and the central phenyl ring seem to play a leading role in the interaction with C_{60} for the three different host systems studied. According to the experimental findings, the benzene ring closer to the triazole ring in the exTTF and TCAQ skeletons also participate in the complexation with the C_{60} unit. These observations are in agreement with that found with host **6**, endowed with phenyl rings at terminal positions. These main contributions to the complex formation might account for the similar binding constants estimated for all host-guest systems.

Theoretical calculations

In order to shed light on the supramolecular complexation between hosts **4**–**6** and guest C_{60}, and to understand the negligible effect of the peripheral tweezer groups into the binding constant, we performed theoretical calculations under the density functional theory (DFT) framework. Due to the high conformational freedom of hosts **4**–**6**, symmetry-restricted C_s geometry optimizations were performed at the B97D/6-31G** level to obtain comparable structures for the different supramolecular complexes.

Several host–guest arrangements were found for the smallest host **6** when bound to C_{60} (**6a–c·C$_{60}$**, Figure 7). In the minimum-energy geometry of **6a·C$_{60}$**, the peripheral benzene arms of the host arrange in an open-like shape, embracing the fullerene guest with a combination of π–π (central and peripheral benzenes; distances **a** and **d**, respectively, in Figure 7) and CH···π (triazole and methylene moieties; **b** and **c**) interactions (Table 2). This supramolecular arrangement is computed with the largest interaction energy (ΔE_{int} = –30.91 kcal/mol) among the different conformations found for **6·C$_{60}$** (Table 3). By displacing the peripheral benzenes away from C_{60}, it is possible to estimate the supramolecular stabilization due to the tweezer core only (**6b·C$_{60}$**), which is predicted to be –23.53 kcal/mol. Finally, another conformer **6c·C$_{60}$**, in which the host wraps itself and covers C_{60} in a crown shape with a series of π–π and CH···π interactions (Table 2), is found also with high stability (ΔE_{int} of –30.58 kcal/mol). The host disposition in **6c·C$_{60}$** is hindered for larger exTTF and TCAQ-based tweezers, and thus a similar conformation is not found in **4–5·C$_{60}$**. Otherwise, supramolecular

assemblies analogous to **6a·C$_{60}$** are obtained as the most stable complexes for **4–5·C$_{60}$** (Figure 7). Compared to **6·C$_{60}$**, the interaction energy notably increases in **4·C$_{60}$** and **5·C$_{60}$** (–51.45 and –49.69 kcal/mol, respectively) as a result of the additional π–π interactions originated between the concave part of the tweezer arms (exTTF or TCAQ) and the convex region of C$_{60}$ (Figure 7 and Table 2).[10a,28] The amount of noncovalent interactions can be visualized by analysis of the noncovalent index (NCI) for the host–guest assemblies (see Figure S26). Theoretical calculations therefore suggest that an extension of the peripheral π-conjugated arms from benzene in **6** to exTTF in **4** and TCAQ in **5** is accompanied by an enhanced interaction with the fullerene guest due to the favourable concave–convex complementarity of the peripheral exTTF and TCAQ units with the C$_{60}$ guest.

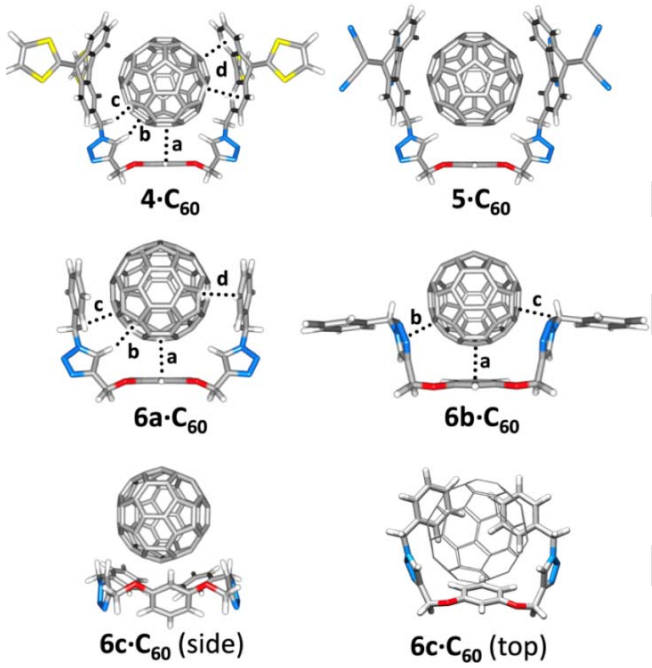

Figure 7. Minimum-energy structures calculated for the tweezer·C$_{60}$ complexes at the B97D/6-31G** level. Characteristic intermolecular distances **a–d** are defined. Side and top (wire fullerene) views are displayed for **6c**•C$_{60}$.

Table 2. Characteristic intermolecular distances **a–d** (in Å) calculated for the tweezer·C$_{60}$ complexes at the B97D/6-31G** level.[a]

	a	b	c	d
4·C$_{60}$	3.23	2.39	2.69	3.00–3.18
5·C$_{60}$	3.22	2.40	3.03	3.02–3.16
6a·C$_{60}$	3.31	2.47	2.59	3.19
6b·C$_{60}$	3.38	3.27[b]	2.64	-
6c·C$_{60}$	3.21	2.47	2.96	3.08

[a] Intermolecular distances **a–d** are defined in Figure 7. [b] π-π interaction between triazole ring and C$_{60}$.

The interaction energy is an accurate descriptor to estimate the binding energy in a supramolecular aggregate when the constituting molecular entities are rigid. However, the energy penalty required for the monomers to acquire their geometry in the complex must be considered when at least one of the moieties presents flexibility. The binding energy (ΔE_{bind}) was therefore calculated as

$$\Delta E_{\mathrm{bind}} = \Delta E_{\mathrm{int}} + E_{\mathrm{def}}$$

where ΔE_{int} and E_{def} are the interaction and deformation energy, respectively (see the Experimental Section for further details). Due to the large conformational space of the molecular tweezers **4–6** and the rigidity of the fullerene moiety, the deformation energy can be ascribed to the host only ($E_{def} \approx E_{def,host}$). Minimum-energy geometries for the isolated hosts **4–6** show that the peripheral arms twist to self-interact (Figure 8a). The NCI analysis predicts a series of intramolecular noncovalent interactions that stabilize the folded conformation compared to the open disposition in the supramolecular complex (Figure 8b, and Figures S27 and S28). The deformation energy is calculated between +1.92 and +10.20 kcal/mol for **6** depending on the conformer (Table 3). Structure **6c** provides the lowest E_{def} value as the favourable intramolecular interactions still remain upon formation of the host–guest complex (Figure S28). Moving to larger hosts **4** and **5**, the deformation energy significantly increases to +19.44 and +19.05 kcal/mol, respectively. This increase in E_{def} results from the large amount of noncovalent interactions that have to be suppressed in going from the minimum-energy geometry of the isolated host to its disposition in the aggregate (see Figure 8b for **4**). The deformation energy therefore counterbalances the large and negative interaction energy calculated in our tweezer·C$_{60}$ complexes, and allows a more accurate determination of the binding energy (ΔE_{bind}). Theoretical binding energies show that the crown-like conformer **6c** provides the larger stability for the benzene-based **6·C$_{60}$** assembly, as a result of the small host deformation penalty, with an ΔE_{bind} of –28.67 kcal/mol (Table 3). Moving to the exTTF and TCAQ tweezers, the binding energy barely increases due to the large and positive E_{def} values, and ΔE_{bind} values of –32.01 and –30.64 kcal/mol are predicted for **4·C$_{60}$** and **5·C$_{60}$**, respectively. Theoretical calculations therefore indicate that the enhanced interaction between hosts **4–6** and the fullerene guest upon increasing the size of the π-conjugated arms of the tweezer is compensated by an increase in the deformation energy penalty. This results into similar binding energies of ca. –30 kcal/mol calculated for the three host-guest assemblies, and allows explaining the negligible effect of the tweezer size into the experimental association constants. The deformation energy penalty also explains the similar values obtained for the association constant of **4–5**•C$_{60}$ compared with structurally related tweezers holding a smaller but more rigid central scaffold.[15]

Table 3. Interaction energy (ΔE_{int}), deformation energy (E_{def}), and binding energy (ΔE_{bind}) (in kcal/mol) calculated for the tweezer·C_{60} assemblies.

Complex	ΔE_{int}	E_{def}	ΔE_{bind}
4·C_{60}	–51.45	+19.44	–32.01
5·C_{60}	–49.69	+19.05	–30.64
6a·C_{60}	–30.91	+8.44	–22.47
6b·C_{60}	–23.53	+10.20	–13.33
6c·C_{60}	–30.58	+1.92	–28.67

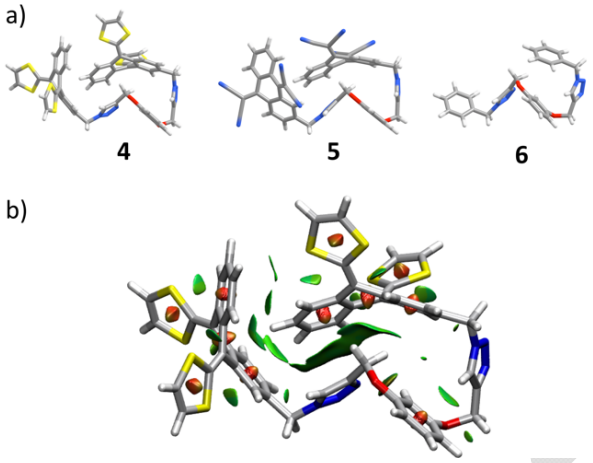

Figure 8. a) Minimum-energy structure calculated for hosts **4–6**. b) NCI isosurfaces obtained for **4**. Green regions indicate stabilizing noncovalent interactions whereas reddish features show steric ring tensions.

Conclusions

The synthesis and characterization of SWCNT and MWCNT nanoconjugates endowed with a tweezer-like receptor based on exTTF was described. The exTTF receptor recognizes C_{60} units both in the free state and when covalently attached to SWCNTs and MWCNTs, with values for the association constant K_a in a range of similar reported hosts (ca. 10^3 M^{-1}).[14] The study was extended to analogous systems based on TCAQ and benzene rings as recognitions motifs. A comprehensive analysis on the nature of the host-guest interaction was performed by ^{1}H NMR and theoretical methods. The three analogous **4–6** hosts, bearing different recognition motifs (exTTF, TCAQ, and phenyl), have similar contributing forces to the overall stability of the system, particularly relevant in ^{1}H NMR titration experiments are the interactions of C_{60} with the central phenyl ring and the C−H in the triazole ring of the hosts. By means of theoretical calculations, the nature of the supramolecular recognition was elucidated, and the negligible effect of the tweezer size into the experimental binding constants was rationalized by a compensation between interaction and deformation energies.

Experimental Section

Materials and General Methods

HiPco SWCNT were purchased from Carbon Nanotechnologies (lot: P0261, purity >82 %, <18 % remaining iron particles, length = 100-1000 nm, diameter = 0.8-1.4 nm) and used without any further purification treatment. MWCNT were synthesized by CVD using Fe/Al_2O_3 as catalyst at 650 °C.[29] The starting MWCNT can attain 10 μm in length and most of them exhibit closed ends. The internal diameter varies between 4 and 12 nm, while the external goes from 8 to 21 nm. Organic solvents and reagents used in this work were purchased from commercial suppliers and used as received, unless stated otherwise. 3,5-bis(propargyloxy)benzyl chloride **1**,[18] 2-(azidomethyl)-9,10-bis-(1,3-dithiol-2-ylidene)-9,10-dihydroanthracene **2**,[19] 2-(azidomethyl)anthraquinone,[26] 5-(chloromethyl)-1,3-bis(((9,10-bis(dicyanomethylidene)-9,10-dihydro-anthracen-2-yl)methyl)-1H-4-(1,2,3-triazolyl)methyloxy) benzene **6**,[18] and **SWCNT-1** and **MWCNT-1**,[16] were synthesized by following the previously reported methods or slightly modified procedures.

General Methods

NMR spectra were recorded on a Bruker Avance 300 spectrometer at 298 K using partially deuterated solvents as internal standards. Coupling constants (J) are denoted in Hz and chemical shifts (δ) in ppm. Multiplicities are denoted as follows: s = singlet, d = doublet, t = triplet, m = multiplet, br = broad. FTIR spectra were carried out using pellets of dispersed samples of the corresponding compounds in dried KBr. The instrument used was a Bruker TENSOR FTIR. The spectral range was 4000-400 cm^{-1}. Matrix-assisted laser desorption ionization (coupled to a time-of-flight analyzer) experiments (MALDI-TOF) were recorded on a Bruker REFLEX spectrometer. Absorption spectra were recorded with a Varian Cary 50 spectrophotometer and a Varian Cary 5000 spectrometer. TGA analyses were carried out under air and nitrogen in a TA-TGA-Q500 apparatus. The sample (~ 0.5 mg) was introduced inside a platinum crucible and equilibrated at 90 ºC followed by a 10 °C min^{-1} ramp between 90 and 1000 °C. XPS analyses were carried out using a SPECS GmbH (PHOIBOS 150 9MCD) spectrometer operating in the constant analyzer energy mode. A non-monochromatic aluminium X-ray source (1486.61 eV) was used with a power of 200 W and voltage of 12 kV. Pass energies of 75 and 25 eV were used for acquiring both survey and high resolution spectra, respectively. Survey data were acquired from kinetic energies of 1487–400 eV with an energy step of 1 eV and 100 ms dwell time per point. The high resolution scans were taken around the emission lines of interest with 0.1 eV steps and 100 ms dwell time per point. SpecsLab Version 2.48 software was used for spectrometer control and data handling. The semi-quantitative analyses were performed from the C 1s (284.3 eV) signal. The samples were introduced as pellets of 8 mm diameter. Raman spectra were recorded on Renishaw in Via Microscope at room temperature using an exciting laser source of 785 nm. TEM micrographs were obtained using a JEOL 2100 microscope operating at 200 kV. The samples were dispersed in DMF, sonicated for 5 minutes, and the resulting suspension dropped onto a holey carbon copper grid (200 mesh), the solvent was allowed to evaporate before analysis.

Theoretical Calculations

Density functional theory calculations were performed to quantify the affinity of our tweezers towards fullerene recognition by using the Gaussian-09.D01 suite of packages.[30] First, we optimized the structure

of the host–guest complexes with the Grimme's dispersion-corrected B97D functional,[31] which has demonstrated a great accuracy-computational cost trade-off.[32] The popular and cost-effective Pople's 6-31G** basis set was used throughout.[33] Note that we do not include the counterpoise correction to the basis set superposition error as there is still debate on its usefulness.[34] Minimum-energy geometries were also obtained for the constituting monomers at the B97D/6-31G** level. Due to the large conformational space of the flexible tweezers, several conformers were optimized, and only the most stable ones are discussed. Symmetry-restricted C_s optimizations, with a symmetry plane cutting perpendicularly the central phenyl ring, were performed to obtain comparable structures between the different complexes. The binding energy (ΔE_{bind}) was calculated according to:

$$\Delta E_{\text{bind}} = \Delta E_{\text{int}} + E_{\text{def}}$$

where ΔE_{int} and E_{def} are the interaction and deformation energy, respectively. ΔE_{int} is the stabilizing energy between the two monomers when combined in the dimer, and is defined as:

$$\Delta E_{\text{int}} = E_{\text{AB}}^{\text{AB}} - E_{\text{A}}^{\text{AB}} - E_{\text{B}}^{\text{AB}}$$

where E_{X}^{Y} denotes the energy of system X at the geometry of system Y, being the system either one of the two monomers A and B or the complex AB. Otherwise, E_{def} is the energy penalty required for the monomers to move from their relaxed geometry to the geometry in the dimer, and is calculated according to:

$$E_{\text{def}} = E_{\text{def,A}} + E_{\text{def,B}} = (E_{\text{A}}^{\text{AB}} - E_{\text{A}}^{\text{A}}) + (E_{\text{B}}^{\text{AB}} - E_{\text{B}}^{\text{B}})$$

The deformation energy in our host–guest complexes mainly arises from the tweezer receptor, which has a large conformational space, whereas fullerene barely contributes due to its rigid skeleton. Thus,

$$E_{\text{def,fullerene}} \approx 0$$

$$E_{\text{def,host}} \approx E_{\text{def}}$$

The noncovalent index (NCI) was calculated for the hosts and host–guest complexes by using the NCIPLOT-3.0 software.[35] The PROMOLECULAR densities were employed, along with density and reduced density gradient thresholds of 0.2 au and 1.0, respectively, and a discarding density parameter of 0.95 au for the intermolecular NCI selection. Geometry structures were represented using the Chemcraft software,[36] whereas the NCI surfaces were plotted through the VMD-1.9.3 program.[37]

Synthesis

5-(Chloromethyl)-1,3-bis(((9,10-di(1,3-dithiol-2-ylidene)-9,10-dihydroanthracen-2-yl)methyl)-1H-4-(1,2,3-triazolyl)methyloxy) benzene (3): A DMSO suspension of **2**[19] (0.150 g, 0.345 mmol), 3,5-bis(propargyloxy)benzyl chloride **1**[18] (0.041 g, 0.173 mmol), $CuBr{\cdot}SMe_2$ (0.014 g, 0.07 mmol), sodium ascorbate (0.009 g, 0.07 mmol), and copper wires were sealed under Ar atmosphere and irradiated under microwave conditions (110 ^{0}C, 850 W) during 2 hours. The resulting dark solution was percolated through a small column containing Quadrasil®MP to remove the remaining copper. Ethanol was then added to precipitate the desired product that after several cycles of centrifugation and washing with EtOH was isolated as a dark yellow solid (65 %). M.p. 275–277 ºC; ^{1}H NMR ($CDCl_3$, 300 MHz): δ = 7.71–7.63 (Ar−H, m, 6H), 7.58 (N−CH, s, 2H), 7.51 (Ar−H, d, 2H, J = 1.3 Hz), 7.31–7.25 (Ar−H, m, 4H), 7.16 (Ar−H, d, 2H, J = 8.1 Hz), 6.59 (Ar−H, s, 2H), 6.55 (Ar−H, s, 1H), 6.27 (S−CH, s, 4H), 6.23 (S−CH, d, 2H, J = 6.7 Hz), 6.18 (S−CH, d, 2H, J = 6.7 Hz), 5.53 (CH_2N, s, 4H), 5.13 (CH_2O, s, 4H), 4.45 (CH_2Cl, s, 2H) ppm; ^{13}C NMR ($CDCl_3$, 75 MHz): δ = 159.6 (ArC−O), 144.4 (C−N), 139.7 (ArC−CH_2Cl), 137.0 (ArC), 136.8 (ArC), 136.3 (ArC), 135.8 (ArC), 135.2 (ArC), 135.1 (ArC), 131.9 (ArC), 126.2 (ArCH), 126. 1(ArCH), 125.6 (ArCH), 125.5 (ArCH), 125.0 (ArCH), 124.9 (ArCH), 124.5 (ArCH), 122.9 (N−CH), 121.4 (ArC−S), 121.1 (ArC−S), 117.4 (SCH), 117.1 (SCH), 108.1 (ArCH), 101.8 (ArCH), 62.3 (CH_2N), 54.2 (CH_2OAr), 46.1 (CH_2Cl) ppm; FTIR (KBr): ν = 3068, 3009, 2926, 2859, 1666, 1599, 1548, 1510, 1457, 1342, 1290, 1157, 1050, 802, 755 cm^{-1}; UV/Vis ($CHCl_3$): λ_{max} = 367, 414, 425 nm; HRMS (MALDI): calcd. for $C_{55}H_{37}ClN_6O_2S_8Na$ 1127.0330; found 1127.0365.

5-(Azidomethyl)-1,3-bis(((9,10-di(1,3-dithiol-2-ylidene)-9,10-dihydroanthracen-2-yl)methyl)-1H-4-(1,2,3-triazolyl)methyloxy) benzene (4): A solution of chloride **3** (0.050 g, 0.05 mmol) and NaN_3 (0.059 g, 0.90 mmol) in THF/water was heated under Ar atmosphere at 70 ^{0}C overnight. The reaction was followed by ^{1}H NMR observing the decrease in the methylene signal at 4.45 ppm and the increase in the signal at 4.22 ppm corresponding to the azidomethyl group. When the CH_2Cl signal disappeared completely, the reaction was allowed to reach r.t. The crude was extracted with $CHCl_3$, dry over $MgSO_4$, filtered, and taken to dryness, yielding the desired product as a dark yellow solid (98 %). M.p. 260–263 ºC; ^{1}H NMR ($CDCl_3$, 300 MHz): δ = 7.71–7.63 (Ar−H, m, 6H), 7.59 (N−CH, s, 2H), 7.53 (Ar−H, d, 2H, J = 1.3 Hz), 7.30–7.25 (Ar−H, m, 4H), 7.18 (Ar−H, d, 2H, J = 8.1 Hz), 6.57 (Ar−H, s, 1H), 6.52 (Ar−H, m, 2H), 6.29 (S−CH, s, 4H), 6.25 (S−CH, d, 2H, J = 6.7 Hz), 6.20 (S−CH, d, 2H, J = 6.7 Hz), 5.54 (CH_2N, s, 4H), 5.15 (CH_2O, s, 4H), 4,22 (CH_2N_3, s, 2H) ppm; ^{13}C NMR ($CDCl_3$, 75 MHz): δ = 159.9 (ArC−O), 144.4 (C−N), 140.8 (ArC−CH_2Cl), 137.1 (ArC), 136.9 (ArC), 136.5 (ArC), 136.0 (ArC), 135.3 (ArC), 135.2 (ArC), 131.9 (ArC), 126.3 (ArCH), 126.2(ArCH), 126.1 (ArCH), 125.7 (ArCH), 125.1 (ArCH), 125.0 (ArCH), 124.7 (ArCH), 123.0 (N−CH), 121.8 (ArC−S), 121.6 (ArC−S), 117.5 (SCH), 117.2 (SCH), 107.8 (ArCH), 101.9 (ArCH), 62.3 (CH_2N), 54.2 (CH_2OAr), 29.9 (CH_2N_3) ppm; FTIR (KBr): ν = 2924, 2856, 2099, 1735, 1597, 1548, 1511, 1459, 1349, 1259, 1217, 1161, 1049, 801, 755 cm^{-1}; UV/Vis ($CHCl_3$): λ_{max} = 369, 416, 423 nm; HRMS (MALDI): calcd. for $C_{55}H_{37}N_9O_2S_8Na$ 1134.0734; found 1134.0647.

2-Azidomethyl-9,10-bis-(dicyamomethylen)anthracene: A solution of 2-(azidomethyl)anthraquinone[26] (0.16 g, 0.61 mmol) and malonitrile (0.10 g, 1.52 mmol) in $CHCl_3$ (50 mL) was heated under Ar atmosphere at 65 ^{0}C. Then, $TiCl_4$ and pyridine were added dropwise, keeping the solution stirring at this temperature 24 hours. The same amounts of malonitrile, $TiCl_4$ and pyridine were added again, and the stirring maintained for another 24 hours. The reaction mixture was left to reach r.t. and filtered over celite, washed with water, dry over Na_2SO_4, and filtered. The crude was taken to dryness and then purified by silica gel column chromatography using a hexane/DCM (2/1) mixture as eluent to yield a yellow solid (90 %). M.p. 292–294 ºC; ^{1}H NMR ($CDCl_3$, 300 MHz): δ = 8.22–8.16 (m, 3H), 8.14 (d, 1H, J = 1.4 Hz), 7.72–7.65 (m, 2H), 7.62 (dd, 1H, J = 8.1 Hz, J = 1.7 Hz), 4.52 (s, 2H) ppm; ^{13}C NMR ($CDCl_3$, 75 MHz): δ = 160.2 (ArC), 160.0 (ArC), 141.5 (C−CH_2N_3), 133.0 (ArCH), 131.9 (ArCH), 131.2 (ArC), 130.5 (ArC), 130.4 (ArC), 128.5 (ArCH), 128.1 (ArCH), 127.1 (ArCH), 113.3 (C≡N), 84.0 (C−C≡N), 83.7 (C−C≡N), 54.1 (CH_2N_3) ppm; FTIR (KBr): ν = 3005, 2970, 2228, 2105, 1589, 1560, 1337, 1282, 1221, 836, 767, 694 cm^{-1}; UV/Vis ($CHCl_3$): λ_{max} = 354 nm; HRMS (MALDI): calcd. for $C_{21}H_9N_7Na$ 382.0817; found : 382.0820.

5-(Chloromethyl)-1,3-bis(((9,10-bis(dicyanomethylidene)-9,10-dihydroanthracen-2-yl)methyl)-1H-4-(1,2,3-triazolyl)methyloxy) benzene (5): A DMSO suspension of 2-azidomethyl-9,10-bis-(dicyamomethylen)anthracene (0.306 g, 0.85 mmol), 3,5-

bis(propargyloxy)benzyl chloride **1**[18] (0.100 g, 0.42 mmol), $CuBr{\cdot}SMe_2$ (0.035 g, 0.17 mmol), sodium ascorbate (0.022 g, 0.17 mmol), and copper wires were sealed under Ar atmosphere and irradiated under microwave conditions (110 ^{0}C, 850 W) during 2 hours. The resulting dark solution was percolated through a small column containing Quadrasil®MP to remove the remaining copper. Ethanol was then added to precipitate the desired product that after several cycles of centrifugation and washing with EtOH was isolated as dark yellow solid (85 %). M.p. 276–280 ºC; ^{1}H NMR ($CDCl_3$, 300 MHz): δ = 8.28–8.21 (Ar−H, m, 6H), 7.95 (N−CH, s, 2H), 7.77–7.74 (Ar−H, m, 6H), 7.61 (Ar−H, dd, 2H, *J* = 8.0 Hz, *J* = 1.5 Hz), 6.62 (Ar−H, d, 2H, *J* = 2.2 Hz), 6.58 (Ar−H, t, 1H, *J* = 2.2 Hz), 5.71 (CH_2N, s, 4H), 5.20 (CH_2O, s, 4H), 4.48 (CH_2Cl, s, 2H) ppm; ^{13}C NMR ($CDCl_3$, 75 MHz): δ = 159.4 (ArC), 159.3 (ArC−O), 145.0 (C−N), 139.7 (ArC−CH_2Cl), 132.7 (ArCH), 131.3 (ArCH), 131.2 (ArC), 130.4 (ArC), 129.9 (ArC), 128.4 (ArCH), 127.7 (ArCH), 126.4 (ArCH), 123.5 (N−CH), 113.1 (C≡N), 113.0 (C≡N), 112.9 (C≡N), 112.8 (C≡N), 108.3 (ArCH), 102. (ArCH), 83.6 (C−C≡N), 62.0 (CH_2N). 53.0 (CH_2OAr), 46.1 (CH_2Cl) ppm; FTIR (KBr): ν = 3145, 3072, 2932, 2228, 1596, 1558, 1459, 1329, 1294, 1225, 1158, 1048, 825, 771, 733, 693 cm^{-1}; UV/Vis ($CHCl_3$): λ_{max} = 353 nm; HRMS (MALDI): calcd. for $C_{55}H_{29}ClN_{14}O_2Na$ 975.2184; found 975.2197.

SWCNT-2: The alkyne functionalized **SWCNT-1**[16] (20 mg) were suspended in NMP (20 mL) with 0.08 mL of tetra-*n*-butylammonium fluoride (TBAF) (1 M in THF) (0.27 µmol) for two hours to cleavage the TMS protecting groups. Subsequently, receptor **4** (0.05 mmol), copper sulfate (3.1 µm), sodium ascorbate (31.3 µm), and some copper wires were added. After 24 hours at 70 °C, the reaction mixture was filtered and washed over a polytetrafluoroethylene (PTFE) membrane several times with NMP, CH_2Cl_2, and MeOH (sonicated, centrifuged, and filtered) until the filtered solution remained colourless to remove the non reacted material. In a second washing step, the solid was washed with water to eliminate the copper catalysts. FTIR (KBr): ν = 2900 (C−H stretching mode) and 1597 (C−H in-plane stretching mode) cm^{-1}; TGA: weight loss and temperature desorption (organic anchoring groups): 40 %, 600 °C; Raman: I_D/I_G = 0.284; XPS: % atomic: C (284.6 eV) = 82.23, O (532.6 eV) = 10.38, N (399.6eV) = 2.91, S (169.6 eV) = 2.69.

MWCNT-2: A NMP (20 mL) solution of **MWCNT-1**[16] (30 mg) containing 0.2 mL of TBAF (1M in THF) (0.27 µmol) was stirred under inert atmosphere for two hours to eliminate the TMS protecting groups. Receptor **4** (0.05 mmol), copper sulfate (3.1 µm), sodium ascorbate (31.3 µm), and some copper wires were added to the previous solution and reacted for 24 hours at 70 °C to obtain the click chemistry resulting product **MWCNT-2**. The reaction mixture was filtered over a PTFE membrane and subsequently washed with NMP, CH_2Cl_2, and MeOH until the filtered solution remained colorless, to remove the non-reacted material. The copper catalyst was removed on a final washing step using water. FTIR (KBr): ν = 2900 (C−H stretching mode) and 1585 (C−H in-plane stretching mode) cm^{-1}; TGA: weight loss and temperature desorption (organic anchoring groups): 49 %, 600 °C; Raman: I_D/I_G = 2.10; XPS: % atomic: C (284.6 eV) = 88.71, O (532.6 eV) = 8.6, N (400.6 eV) = 1.47, S (164.6 eV) = 1.46.

Acknowledgements

Financial support from the European Research Council (ERC 320441-Chir*all*carbon), MINECO of Spain (CTQ2017-83531-R, CTQ2017-84327-P, and CTQ2015-71154-P) the Generalitat Valenciana (PROMETEO/2016/135), and European Feder funds (CTQ2015-71154-P) is acknowledged. J.C. acknowledges the Generalitat Valenciana for the APOSTD/2017/081 post-doctoral fellowship.

Keywords: carbon nanotubes • density functional calculations • fullerenes • host-guest interactions • π-extended tetrathiafulvalene.

[1] a) H. W. Kroto, J. R. Heath, S. C. O'Brien, R. F. Curl, R. E. Smalley, *Nature* **1985**, *318*, 162–163; b) S. Iijima, *Nature* **1991**, *354*, 56–58; c) S. Iijima, T. Ichihashi, *Nature* **1993**, *363*, 603–605; d) D. S. Bethune, C. H. Klang, M. S. de Vries, G. Gorman, R. Savoy, J. Vazquez, R. Beyers, *Nature* **1993**, *363*, 605–607.

[2] a) M. Bühl, A. Hirsch, *Chem. Rev*. **2001**, *101*, 1153–1184; b) W. Linert, I Lukovits, *J. Chem. Inf. Model*. **2007**, *47*, 887–890; c) G. Povie, Y. Segawa, T. Nishihara, Y. Miyauchi, K. Itami, *Science* **2017**, *356*, 172–175.

[3] a) D. M. Guldi, N. Martín, *Carbon Nanotubes and Related Structures*, Wiley-VCH, Weinheim, 2010; b) V. Georgakilas, J. A. Perman, J. Tucek, R. Zboril, *Chem. Rev.* **2015**, *115*, 4744–4822; c) M. Antonietti, K. Mullen, *Chemical Synthesis and Applications of Graphene and Carbon Materials*, Wiley-VCH, Weinheim, 2016.

[4] a) A. Hirsch, *Fullerenes and Related Structures*, *Top. Curr. Chem.* Springer-Verlag, Berlin-Heidelberg, 1999; b) D. Tasis, N. Tagmatarchis, A. Bianco, M. Prato, *Chem. Rev.* **2006**, *106*, 1105–1136; c) P. Singh, S. Campidelli, S. Giordani, D. Bonifazi, A. Bianco, M. Prato, *Chem. Soc. Rev*. **2009**, *38*, 2214–2230; d) K. Dirian, M. A. Herranz, G. Katsukis, J. Malig, L. Rodríguez-Pérez, C. Romero-Nieto, V. Strauss, N. Martín and D. M. Guldi, *Chem. Sci.* **2013**, *4*, 4335–4353; e) E. Vázquez, F. Giacalone, M. Prato, *Chem. Soc. Rev.* **2014**, *43*, 58–69; f) A. J. Clancy, M. K. Bayazit, S. A. Hodge, N. T. Skipper, C. A. Howard, M. S. P. Shaffer, *Chem. Rev*. **2018**, *118*, 7363–7408.

[5] F. Wang, T. M. Swager, J. *Am. Chem. Soc.* **2011**, *133*, 11181–11193.

[6] a) D. Canevet, E. M. Pérez, N. Martín, *Angew. Chem. Int. Ed.* **2011**, *50*, 9248−9259*; Angew. Chem.* **2011**, *123*, 9416–9427; b) C. García-Simón, M. Costas, X. Ribas, *Chem. Soc. Rev.* **2016**,*45*, 40–62.

[7] a) K. Tashiro, T. Aida, *Chem. Soc. Rev.* **2007**, *36*, 189–197; b) L. Moreira, J. Calbo, B. M. Illescas, J. Aragó, I. Nierengarten, B. Delavaux-Nicot, E. Ortí, N. Martín, J.-F. Nierengarten, *Angew. Chem. Int. Ed.* **2015**, *54*, 1255–1260; *Angew. Chem.* **2015**, *127*, 1271–1276; c) L. Moreira, J. Calbo, J. Aragó, B. M. Illescas, I. Nierengarten, B. Delavaux-Nicot, E. Ortí, N. Martín, J.-F. Nierengarten, *J. Am. Chem. Soc.* **2016**, *138*, 15359–15367; d) M. Ortiz, S. Cho, J. Niklas, S. Kim, O. G. Poluektov, W. Zhang, G. Rumbles, J. Park, *J. Am. Chem. Soc.* **2017**, *139*, 4286–4289.

[8] a) I. Sanchez-Molina, C. G. Claessens, B. Grimm, D. M. Guldi, T. Torres, *Chem. Sci.* **2013**, *4*, 1338−1344; b) S. Nakano, Y. Kage, H. Furuta, N. Kobayashi, S. Shimizu, *Chem. Eur. J.* **2016**, *22*, 7706–7710.

[9] K. Yoshida, A. Osuka, *Chem. Eur. J.* **2016**, *22*, 9396–9403.

[10] a) E. M. Pérez, M. Sierra, L. Sánchez, R. Torres, R. Viruela, P. M. Viruela, E. Ortí, N. Martín*, Angew. Chem. Int. Ed.* **2007**, *46*, 1847–1851; *Angew. Chem.* **2007**, *119*, 1879–1883; b) M. Yamada, K. Ohkubo, M. Shionoya, S. Fukuzumi, *J. Am. Chem. Soc.* **2014**, *136*, 13240–13248; c) Y.-M. Liu, D. Xia, B.-W. Li, Q-Y. Zhang, T. Sakurai, Y.-Z. Tan, S. Seki, S.-Y. Xie, L.-S. Zheng, *Angew. Chem. Int. Ed.* **2016**, *55*, 13047–13051; *Angew. Chem.* **2016**, *128*, 13241–13245.

[11] a) A. Sygula, F. R. Fronczek, R. Sygula, P. W. Rabideau, M. M. Olmstead, *J. Am. Chem. Soc.* **2007**, *129*, 3842–3843; b) M. Takeda, S. Hiroto, H. Yokoi, S. Lee, D. Kim, H. Shinokubo, *J. Am. Chem. Soc.* **2018**, *140*, 6336–6342.

[12] a) T. Kawase, K. Tanaka, N. Shiono, Y. Seirai, M. Oda*, Angew. Chem. Int. Ed.* **2014**, *43*, 1722–1724; *Angew. Chem.* **2014**, *116*, 1754–1756; b) Y. Lu, Z.-D. Fu, Q.-H. Guo, M.-X. Wang*, Org. Lett*. **2017**, *19*, 1590–1593.

[13] a) Y. Inokuma, T. Arai, M. Fujita, *Nat. Chem.* **2010**, *2*, 780–783; b) Y. Shi, K. Cai, H. Xiao, Z. Liu, J. Zhou, D. Shen, Y. Qiu, Q.-H. Guo, C. Stern, M. R. Wasielewski, F. Diederich, W. A. Goddard, J. F. Stoddart, *J. Am. Chem. Soc.* **2018**, *140*, 13835–13842.

[14] a) E. M. Pérez, L. Sánchez, G. Fernández, N. Martín, *J. Am. Chem. Soc.* **2006**, *128*, 7172–7173, b) H. Isla, M. Gallego, E. M. Pérez, R. Viruela, E. Ortí, N. Martín, *J. Am. Chem. Soc.* **2010**, *132*, 1772–1773; c) E. M. Pérez, N. Martín, *Chem. Soc. Rev.* **2015**, *44*, 6425–6433.

[15] E. M. Pérez, A. L. Capodilupo, G. Fernández, L. Sánchez, P. M. Viruela, R. Viruela, E. Ortí, M. Bietti, N. Martín, *Chem. Commun.* **2008**, 4567–4569.

[16] J. Mateos-Gil, L. Rodríguez-Pérez, M. Moreno Oliva, G. Katsukis, C. Romero-Nieto, M. A. Herranz, D. M. Guldi, N. Martín, *Nanoscale* **2015**, *7*, 1193–1200.

[17] a) C. Romero-Nieto, R. García, M. A. Herranz, L. Rodríguez-Pérez, M. Sánchez-Navarro, J. Rojo, N. Martín, D. M. Guldi, *Angew. Chem. Int. Ed.* **2013**, *52*, 10216–10220; *Angew. Chem.* **2013**, *125*, 10406–10410; b) R. García, J. Calbo, R. Viruela, M. A. Herranz, E. Ortí, N. Martín, *ChemPlusChem* **2018**, *83*, 300–307.

[18] P. Wu, A. K. Feldman, A. K. Nugent, C. J. Hawker, A. Scheel, B. Voit, J. Pyun, J. M. J. Fréchet, K. B. Sharpless, V. V. Fokin, *Angew. Chem. Int. Ed.* **2004**, *43,* 3928–3932; *Angew. Chem.* **2004**, *116*, 4018–4022.

[19] S. González, N. Martín, A. Swartz and D. M. Guldi, *Org. Lett.* **2003**, *5*, 557–560.

[20] H. Iden, F. G. Fontaine, J. F. Morin, *Org. Biomol. Chem.* **2014**, *28*, 4117–4123.

[21] M.S. Dresselhaus, G. Dresselhaus, R. Saito, A. Jorio, *Phys. Rep.* **2005**, *409*, 47–99.

[22] T. I. T. Okpalugo, P. Papakonstantinou, H. Murphy, J. McLaughlin, N. M. D. Brown, *Carbon* **2005**, *43*, 153–154.

[23] S. Ciampi, T. Böcking, K. A. Kilian, M. James, J. B. Harper, J. J. Gooding, *Langmuir*, **2007**, *23*, 9320–9329.

[24] a) J. N. Weiss, *FASEB J.,* **1997**, *11*, 835-841; b) K. A. Connors, *Binding Constants: The Measurement of Molecular Complex Stability,* Wiley-VCH, Weinheim, 1987.

[25] To check if this finding may be caused by effect of dilution or precipitation during the experiment, a blank titration using pristine SWCNT instead of **SWCNT-2**, as well as dilution experiments, were performed and a different behaviour was observed.

[26] a) W. Lehnert, *Tetrahedron Lett.* **1970**, *11*, 4723–4724; b) W. Lehnert, *Synthesis*, **1974**, 667–669.

[27] E. L. Myers, R. T. Raines, *Angew. Chem. Int. Ed.* **2009**, *48,* 2359–2363; *Angew. Chem.* **2009**, *121*, 2395–2399.

[28] a) N. Martín, E. M. Pérez, *Chem. Soc. Rev*. **2008**, *37*, 1512–1519; b) J. Calbo, J. C. Sancho-García, E. Ortí, J. Aragó, *Molecules* **2018**, *23*, 118; c) J. Calbo, J. Aragó, R. A. Boto, J. Sánchez-Marín, E. Ortí, J. Contreras-García, *J. Phys. Chem. A*, **2018**, *122*, 1124–1137.

[29] M. Corrias, B. Caussat, A. Ayral, J. Durand, Y. Kihn, P. Kalck, P. Serp, *Chem. Eng. Sci*. **2003**, *58*, 4475–4482.

[30] Gaussian 09, Revision D.01, M. J. Frisch, G. W. Trucks, H. B. Schlegel, G. E. Scuseria, M. A. Robb, J. R. Cheeseman, G. Scalmani, V. Barone, G. A. Petersson, H. Nakatsuji, X. Li, M. Caricato, A. V. Marenich, J. Bloino, B. G. Janesko, R. Gomperts, B. Mennucci, H. P. Hratchian, J. V. Ortiz, A. F. Izmaylov, J. L. Sonnenberg, D. Williams-Young, F. Ding, F. Lipparini, F. Egidi, J. Goings, B. Peng, A. Petrone, T. Henderson, D. Ranasinghe, V. G. Zakrzewski, J. Gao, N. Rega, G. Zheng, W. Liang, M. Hada, M. Ehara, K. Toyota, R. Fukuda, J. Hasegawa, M. Ishida, T. Nakajima, Y. Honda, O. Kitao, H. Nakai, T. Vreven, K. Throssell, J. A. Montgomery, Jr., J. E. Peralta, F. Ogliaro, M. J. Bearpark, J. J. Heyd, E. N. Brothers, K. N. Kudin, V. N. Staroverov, T. A. Keith, R. Kobayashi, J. Normand, K. Raghavachari, A. P. Rendell, J. C. Burant, S. S. Iyengar, J. Tomasi, M. Cossi, J. M. Millam, M. Klene, C. Adamo, R. Cammi, J. W. Ochterski, R. L. Martin, K. Morokuma, O. Farkas, J. B. Foresman, and D. J. Fox, Gaussian, Inc., Wallingford CT, **2016.**

[31] a) S. Grimme, *J. Comput. Chem.* **2006**, *27*, 1787–1799; b) S. Grimme, S. Ehrlich, L. Goerigk, *J. Comput. Chem.* **2011**, *32*, 1456–1465.

[32] L. Goerigk, H. Kruse, S. Grimme, *ChemPhysChem* **2011**, *12*, 3421–3433.

[33] R. Ditchfield, W. J. Hehre, J. A. Pople, *J. Chem. Phys.* **1971**, *54*, 724–728.

[34] X. W. Sheng, L. Mentel, O. V. Gritsenko, E. J. Baerends, *J. Comput. Chem.* **2011**, *32*, 2896–2901.

[35] a) E. R. Johnson, S. Keinan, P. Mori-Sánchez, J. Contreras-García, A. J. Cohen, W. Yang, *J. Am. Chem. Soc.* **2010**, *132*, 6498–6506; b) J. Contreras-García, E. R. Johnson, S. Keinan, R. Chaudret, J.-P. Piquemal, D. N. Beratan, W. Yang, *J. Chem. Theory Comput.* **2011**, *7*, 625–632.

[36] G. A. Zhurko, *Chemcraft–graphical program for visualization of quantum chemistry computations*. Ivanovo, Russia. https://chemcraftprog.com

[37] W. Humphrey, A. Dalke, K. Schulten, *J. Mol. Graph.* **1996**, *14*, 33–38.

FULL PAPER

Catching the ball with molecules and nanomaterials: The intermolecular forces contributing to the overall stability of complexes formed by triazole tweezer-type receptors and C_{60} are analyzed by ^1H NMR titrations and theoretical methods. These forces allow the construction of sophisticated three-component assemblies where receptors anchored to carbon nanotubes sidewalls recognize C_{60} units.

Jaime Mateos-Gil, Joaquín Calbo, Laura Rodríguez-Pérez, Mª Ángeles Herranz, Enrique Ortí,* and Nazario Martín**

Carbon Nanotubes Conjugated with Triazole-Based Tetrathiafulvalene-Type Receptors for C_{60} Recognition